Solid-State Electronics 56 (2011) 79–84

Contents lists available at ScienceDirect

Solid-State Electronics

journal homepage: www.elsevier.com/locate/sse

Thermal measurements and analysis of AlGaInP/GaInP MQW red LEDs with different chip sizes and substrate thicknesses

H.K. Lee [a], D.H. Lee [a], Y.M. Song [b], Y.T. Lee [b], J.S. Yu [a,*]

[a] Department of Electronics and Radio Engineering, Kyung Hee University, 1 Seocheon-dong, Giheung-gu, Yongin 446-701, Republic of Korea
[b] Department of Information and Communications, Gwangju Institute of Science and Technology, Gwangju 500-712, Republic of Korea

ARTICLE INFO

Article history:
Received 24 April 2010
Received in revised form 4 August 2010
Accepted 16 October 2010
Available online 13 November 2010

The review of this paper was arranged by Prof. E. Calleja

Keywords:
Light emitting diodes
AlGaInP/GaInP
Thermal analysis
Junction temperature

ABSTRACT

Thermal properties of AlGaInP/GaInP MQW red LEDs are investigated by thermal measurements and analysis for different chip sizes and substrate thicknesses. To extract the thermal resistance (R_{th}), junction temperature (T_j) is experimentally determined by both forward voltage and electroluminescence (EL) emission peak shift methods. For theoretical thermal analysis, thermal parameters are calculated in simulation using measured heat source densities. The T_j value increases with increasing the injection current, and it decreases as the chip size becomes larger. The use of a thin substrate improves the heat removal capability. At 450 mA, the T_j values of 315 K and 342 K are measured for 500×500 μm^2 LEDs with 110 μm and 350 μm thick substrates, respectively. For 500×500 μm^2 LEDs with 110 μm thick substrate, the R_{th} values of 13.99 K/W and 14.89 K/W are obtained experimentally by the forward voltage and EL emission peak shift methods, respectively. The theoretically calculated value is 13.44 K/W, indicating a good agreement with the experimental results.

1. Introduction

AlGaInP-based light emitting diodes (LEDs), which cover a broad wavelength spectrum from yellow green to red, have been widely used as a light source for various applications of displays, traffic signals, signs, and general lightings [1–3]. Recently, the progress in material growth, LED structure, and chip processing technology including window/current spreading layers, reflectors, electrode design, and surface roughening has significantly improved the device performance [4–8]. Nevertheless, further efforts towards the realization of high-power AlGaInP-based LEDs are still required for many practical applications. To achieve high output power, the LEDs should operate under high injection current. However, high electrical power increases the junction temperature (T_j) of LEDs due to the enhanced internal device heating. The temperature rise in the junction is the primary cause to degrade the optical output power, reliability, and lifetime of LEDs. Thus, the T_j is a key factor in analyzing the thermal performance of LEDs and it should be measured effectively for a variety of different structures.

The T_j can be experimentally measured by using the forward voltage method, micro-Raman spectroscopy, electroluminescence (EL), and photoluminescence [9–13]. The internal temperature change of LEDs with injection current, which is caused by the self heating effect, can be accurately predicted. Furthermore, thermal simulation makes it possible to get a better understanding of the thermal behaviors of LEDs. Although many studies have investigated the thermal characteristics of GaN-based blue LEDs, there were relatively few reports on the detailed thermal analysis of red LEDs based on AlGaInP materials. Furthermore, the investigation on the thermal analysis of AlGaInP LEDs with vertical electrodes is very useful for vertical LED structures. In this paper, we studied systematically the thermal characteristics of AlGaInP/GaInP multiple quantum well (MQW) red LEDs with different chip sizes for 110 μm and 350 μm thick substrates. Thermal resistance (R_{th}) as well as junction temperature was experimentally and theoretically investigated.

2. Device structure and thermal modelling

Fig. 1 shows the schematic diagram of AlGaInP/GaInP MQW red LEDs with vertical electrodes employed in this experiment. The AlGaInP/GaInP LED structure was grown on a 350 μm thick n-GaAs substrate by using metal organic chemical vapour deposition. After growth of a 0.2 μm thick n-GaAs buffer layer, a 1.2 μm thick n-AlAs/AlGaAs distributed Bragg reflector (DBR) was grown. The 0.7 μm thick 20 pairs of u-AlGaInP/GaInP MQWs were embedded between a 1 μm thick n-$(Al_xGa_{1-x})_{0.5}In_{0.5}P$ layer and a p-type cladding layer. The p-type cladding layer was composed of a 0.7 μm thick AlInP layer and a 0.323 μm thick p-$(Al_xGa_{1-x})_{0.5}In_{0.5}P$ layer, followed by a 0.03 μm thick AlGaInP tensile strain barrier reducing (TSBR) layer, and then it was completed by a 9 μm thick

* Corresponding author. Tel.: +82 31 201 3820; fax: +82 31 206 2820.
E-mail address: jsyu@khu.ac.kr (J.S. Yu).

0038-1101/$ - see front matter © 2010 Elsevier Ltd. All rights reserved.
doi:10.1016/j.sse.2010.10.007

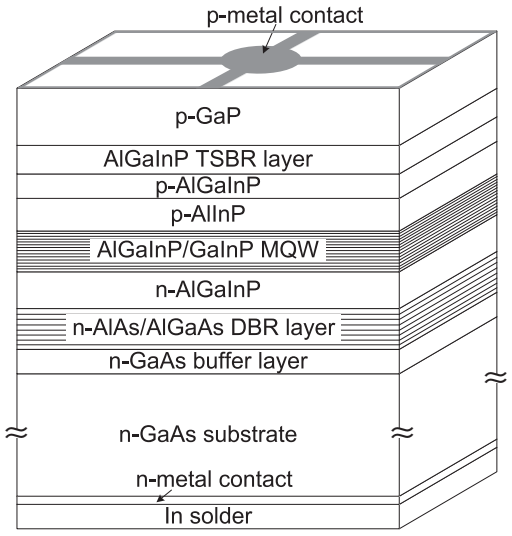

Fig. 1. Schematic diagram of AlGaInP/GaInP MQW red LEDs with vertical electrodes employed in this experiment.

p-GaP window layer. The wafers were processed into LEDs with different chip sizes of $300 \times 300\ \mu m^2$, $400 \times 400\ \mu m^2$, and $500 \times 500\ \mu m^2$. The mesa structures were formed by using inductively coupled plasma (ICP) etcher in $SiCl_4$/Ar plasma. After that, the p electrode of Au/AuBe was deposited on p side by using e-beam evaporator. For some devices, the n-GaAs substrate was lapped and polished up to the thickness of ~110 μm. Then, the n electrode of AuGe/Ni/Au was formed on n side. Finally, the devices were annealed by using rapid thermal annealing in an N_2 ambient at 500 °C for 1 min to form ohmic contacts. For characterization, the fabricated LEDs were bonded on copper heatsink using indium solder and they were wire-bonded to an external contact pad with gold (Au) wire to inject the current. The prepared samples were characterized at various heatsink temperatures. Depending on the monitored temperature by a thermistor located in close proximity to the device, the temperature of LEDs was controlled on the thermoelectric cooler stage.

Thermal analysis of LEDs was carried out theoretically by finite element method (FEM) simulation using a steady-state 3D heat dissipation model. From measured heat source densities, the thermal parameters, such as junction temperature, temperature distribution, heat flux, and thermal resistance, were theoretically simulated for different chip sizes and substrate thicknesses. To simplify the simulation model, the uniform heat generation was assumed within the active region. The generated heat is transferred by three heat transfer mechanisms, i.e., conduction, convection, and radiation. The steady-state ($\partial/\partial t = 0$) 3D heat conduction equation is represented by [14]:

$$-k\left[\frac{\partial^2 T}{\partial x^2}+\frac{\partial^2 T}{\partial y^2}+\frac{\partial^2 T}{\partial z^2}\right]=Q, \quad (1)$$

where k is the thermal conductivity of the constituent materials, Q is the heat source density, and T is the temperature. The heat is partly transferred through the device surfaces in the air by convection and radiation. But the radiation heat transfer can be neglected because it is not primary heat transfer mechanism in this simulation. At boundaries between device surfaces and air, the convection heat transfer can be calculated by the following equation [14]:

$$k\left[\frac{\partial T}{\partial x}+\frac{\partial T}{\partial y}+\frac{\partial T}{\partial z}\right]=h(T_{\mathrm{inf}}-T), \quad (2)$$

Table 1
Thermal conductivities of the constituent materials for AlGaInP/GaInP MQW red LEDs at 298 K [18–20].

Name	Material	Thermal conductivity (W/m K)	Thickness (μm)
p-Electrode	Au/AuBe	315	0.5/0.15
p-Window layer	GaP	77	9
TSBR layer	AlGaInP	177	0.03
p-Cladding layer	$(Al_{0.3}Ga_{0.7})_{0.5}InP$/ $(Al_{0.7}Ga_{0.3})_{0.5}InP$	8.2/5.6	0.023/0.3
	AlInP	76.2	0.7
Active layer (20 pair)	GaInP/AlGaInP MQW	k_L = 10.2, k_V = 8.6	0.7
n-Cladding layer	$(Al_{0.7}Ga_{0.3})_{0.5}InP$/ $(Al_{0.5}Ga_{0.5})_{0.5}InP$	5.6/6.6	0.5/0.5
n-DBR	AlAs/AlGaAs	k_L = 53.6, k_V = 20.3	1.2
n-Buffer layer	GaAs	44	0.2
n-Substrate	GaAs	44	110 (350)
n-Electrode	AuGe/Ni/Au	315	0.12/0.03/0.3
Solder	In	81.6	3
Heatsink	Cu	400	–

where h is the convection heat transfer coefficient and T_{inf} is the ambient temperature.

The QWs and DBRs consist of multilayer thin-film structures. Compared to those of bulk materials, the thermal conductivities in QW and DBR structures should be modified due to the phonon confinement and interface effects [15,16]. For accurate thermal analysis, effective anisotropic thermal conductivities were considered in QW and DBR structures. The thermal conductivities of K_L in lateral direction and K_V in vertical direction are lower than those of bulk materials. Effective anisotropic thermal conductivity can be calculated by a formula related to the thickness and thermal conductivity of constituent materials [17]. Table 1 shows the thermal conductivities of the constituent materials for AlGaInP/GaInP MQW red LEDs at 298 K. For all layers except for the QWs and DBRs, the isotropic thermal conductivities were used. Also, the thermal conductivity of electrodes was assumed as a value of Au.

3. Results and discussion

Fig. 2a shows the voltage–current–light (V–I–L) curves of LEDs with $300 \times 300\ \mu m^2$, $400 \times 400\ \mu m^2$ and $500 \times 500\ \mu m^2$ chip sizes for 110 μm thick substrate at 298 K under continuous-wave (CW) mode. For comparison, the V–I and I–L data of $500 \times 500\ \mu m^2$ LEDs with 350 μm thick substrate are also shown by dashed lines. As the injection current increased, the light output power of LEDs was linearly increased until its saturation began to occur. For larger chip size, the output power was increased distinctly at higher current level. At 480 mA, the output powers of 19.6 mW and 28.9 mW were obtained for $300 \times 300\ \mu m^2$ and $500 \times 500\ \mu m^2$ LEDs, respectively. The forward voltage was slightly decreased as the chip size became larger due to more surface states [21]. The turn-on voltage was also decreased from 1.81 V for $300 \times 300\ \mu m^2$ to 1.75 V for $500 \times 500\ \mu m^2$. For $500 \times 500\ \mu m^2$ chip size, the LED with a thin substrate of 110 μm emitted the higher output power under higher current as shown in Fig. 2a. At injection currents less than 240 mA, two LEDs show similar device characteristics. However, the output power was reduced above 240 mA for the LED with 350 μm thick substrate because of its enhanced internal device heating at higher current. At 480 mA, the output power was 25.1 mW for 350 μm thick substrate. The use of a thin substrate of 110 μm improved the output power by 15.1% compared to the 350 μm thick substrate.

Fig. 2b shows the CW V–I–L curves of the $500 \times 500\ \mu m^2$ LED with 110 μm thick substrate at various heatsink temperatures. The output power was 30.3 mW at 288 K and then it decreased

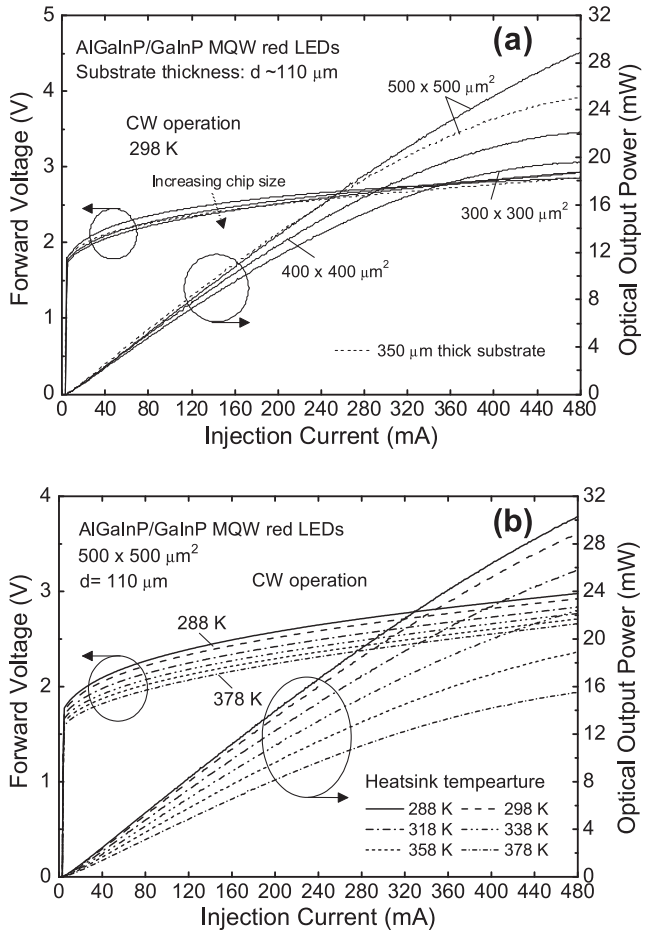

Fig. 2. CW *V–I–L* curves of LEDs (a) with $300 \times 300\ \mu m^2$, $400 \times 400\ \mu m^2$ and $500 \times 500\ \mu m^2$ chip sizes at 298 K and (b) with $500 \times 500\ \mu m^2$ chip size at various heatsink temperatures. The substrate thickness is 110 μm. The dashed lines in (a) show the *V–I* and *I–L* data of $500 \times 500\ \mu m^2$ LEDs with 350 μm thick substrate for comparison.

up to 15.5 mW at 378 K. The forward voltage became lower due to the enhanced leakage current caused by the device heating as the heatsink temperature was increased. The turn-on voltage was reduced from 1.77 V at 288 K to 1.58 V at 378 K. The differential series resistance was kept as 12.3–13.4 Ω at high currents.

Fig. 3 shows the normalized EL intensity versus heatsink temperature for LEDs with different chip sizes at 100 mA in CW operation. The EL intensity was decreased with the increase in heatsink temperature. From the measured EL intensities at 298–378 K, the temperature dependence of the emission intensity (I) can be described by a relationship of $I \propto \exp[-(T - 298\ K)/T_1]$, where T is the heatsink temperature and T_1 is the characteristic temperature [22]. Thus, the relatively low temperature dependence of LEDs leads to a higher characteristic temperature. The T_1 value was increased for larger chip size as shown in Fig. 3. For 110 μm thick substrate, the T_1 values were obtained as 303.8 K, 386.6 K, and 469.8 K for $300 \times 300\ \mu m^2$, $400 \times 400\ \mu m^2$, and $500 \times 500\ \mu m^2$ LEDs, respectively. Also, the T_1 value was substantially reduced by 255.8 K for $500 \times 500\ \mu m^2$ LED with 350 μm thick substrate owing to the increased internal heating. The normalized EL intensity as a function of heatsink temperature for the LED with $500 \times 500\ \mu m^2$ at different injection currents for 110 μm thick substrate is shown in the inset of Fig. 3. As the injection current was increased, both EL intensity and T_1 value were reduced as a result of Joule heating. The T_1 values were measured as 753.8 K, 469.8 K, and 372.7 K at 50 mA, 100 mA, and 150 mA, respectively.

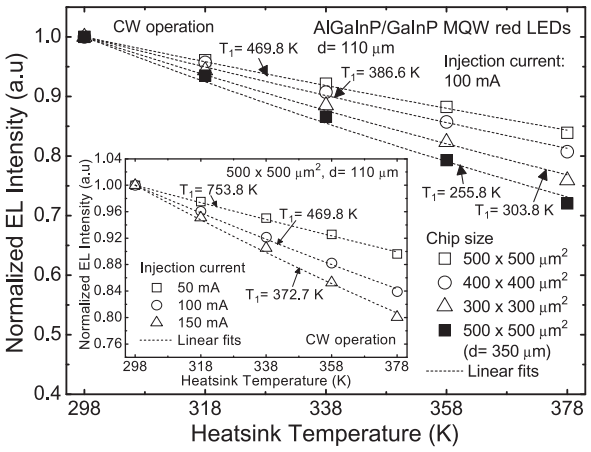

Fig. 3. Normalized EL intensity versus heatsink temperature for LEDs with different chip sizes at 100 mA in CW operation. The inset shows the normalized EL intensity as a function of heatsink temperature for the LED with $500 \times 500\ \mu m^2$ at different injection currents for 110 μm thick substrate.

To measure experimentally the junction temperature of LEDs, the forward voltage and emission peak shift methods were employed. By using the forward voltage method, the T_j can be estimated by the pulsed V_f calibration measurement and DC V_f measurement using a relation, i.e., the difference of the final forward voltage (V_{Ff}) in thermal equilibrium from the initial forward voltage (V_{F0}) divided by the temperature coefficient (K_T) [9]. The K_T value was calculated from the forward voltage change divided by the ambient temperature change. The V_f calibration measurement was carried out under pulsed current with 0.1% duty cycle and 1 μm pulse width because the heating effects are negligible under this condition. The devices were located in a temperature controlled oven. The ambient temperature was changed from 288 K to 378 K with a spacing of 20 K. The K_T values were −2.31 mV/K, −2.56 mV/K, and −2.56 mV/K for 300×300, 400×400, and $500 \times 500\ \mu m^2$ LEDs with 110 μm thick substrate, respectively. For 350 μm thick substrate, the $500 \times 500\ \mu m^2$ LED exhibited a value of $K_T = -2.7$ mV/K.

Fig. 4 shows the measured forward voltage variation of the $500 \times 500\ \mu m^2$ LED with 110 μm thick substrate at 298 K in CW operation for an injection current 60 mA. The forward voltage variation at different injection currents is also shown in the inset of Fig. 4. The forward voltage was measured for 30 min. At $t = 0$ s,

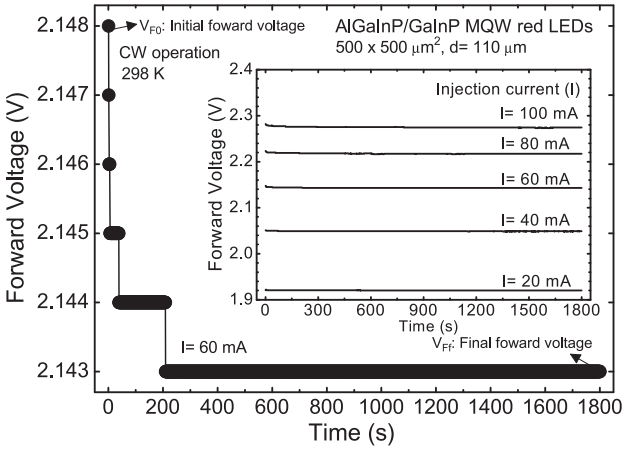

Fig. 4. Measured forward voltage variation of the $500 \times 500\ \mu m^2$ LED with 110 μm thick substrate at 60 mA and at 298 K in CW operation. The inset shows the forward voltage variation at different injection currents.

the forward voltage indicates a V_{F0} and the heating is negligibly small at this point. The forward voltage was rapidly decreased for 200 s after the device was turned on, and then it was stabilized at a constant value when the enough time passed. At t = 1800 s, the forward voltage was measured as a V_{Ff} in thermal equilibrium. As shown in Fig. 4, the V_{F0} was 2.148 V and the V_{Ff} was measured as a constant value of 2.143 V at t = 1800 s. The forward voltage was raised gradually with the increase of injection current. At 20 mA, the forward voltage variation of $|V_{Ff} - V_{F0}|$ was 2.56 mV, and it was increased by 8 mV at 100 mA.

Fig. 5a shows the heat source density versus injection current for LEDs with different chip sizes for 100 and 350 μm thick substrates. The heat source density (Q) generated in active region was obtained from the experimentally measured L–I–V data. The Q values were increased as the more current was injected into the device. For 500 × 500 μm^2 LED with 110 μm thick substrate, the heat source density of $Q = 2.13 \times 10^{12}$ W/m^3 was obtained at 20 mA and it was increased by 7.26×10^{12} W/m^3 at 450 mA. The heat source density was also increased as the chip size became smaller. For 300 × 300 μm^2 LED, the Q value was measured as 6.29×10^{12} W/m^3 and 2.01×10^{13} W/m^3 at 20 mA and 450 mA, respectively. As shown in Fig. 5a, the LEDs with different substrate thicknesses had similar Q values. Above 150 mA, the Q value of 500 × 500 μm^2 LED with 350 μm thick substrate was slightly decreased compared to the device with 110 μm thick substrate due to the reduced forward voltage caused by higher Joule heating. For 500 × 500 μm^2 LED with 350 μm thick substrate, the Q value was 7.12×10^{12} W/m^3 at 450 mA. Fig. 5b shows the heat flux and temperature distribution for the 300 × 300 μm^2 LED with 110 μm thick substrate at 100 mA in CW operation. The temperature is 298 K. The arrow indicates a vector quantity for the heat flux rate (W/m^2). Most of heat is transferred from the active region via the GaAs substrate to copper heatsink by conduction because the heatsink is controlled to a constant temperature of 298 K. For thinner substrate, the generated heat is easily removed because of its shorter heat transfer path.

Fig. 6a shows the measured and simulated junction temperatures versus injection current for LEDs with different chip sizes at 298 K under CW mode. The T_j was experimentally obtained as mentioned above and it was linearly increased with increasing the injection current. For smaller chip size, the T_j became higher. This is certainly attributed to the increased heat source density as can be seen in Fig. 5a. At 100 mA, the measured T_j values were 306.6 K and 301.4 K for 300 × 300 μm^2 and 500 × 500 μm^2 LEDs, respectively. For 500 × 500 μm^2 LED with 350 μm thick substrate, the T_j was increased up to 305.9 K. The LED with 350 μm thick substrate exhibited higher T_j values because its thicker substrate limits the heat dissipation capability. Fig. 6b shows the measured and simulated temperature variations (ΔT) versus dissipated electrical power for 500 × 500 μm^2 LEDs with 110 μm and 350 μm thick substrates. The ΔT values indicated a linear relation with the dissipated electrical power. From these results, the R_{th} was extracted by performing the linear fits (dashed lines). As shown in Fig. 6b, the

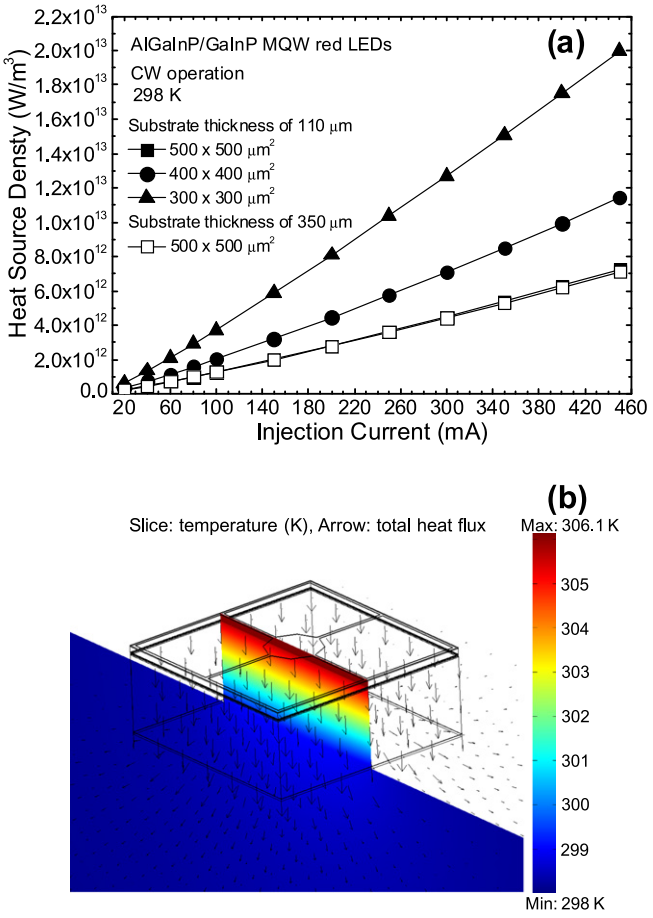

Fig. 5. (a) Heat source density versus injection current for LEDs with different chip sizes for 100 and 350 μm thick substrates and (b) heat flux and temperature distribution for the 300 × 300 μm^2 LED with 110 μm thick substrate at 100 mA and at 298 K in CW operation.

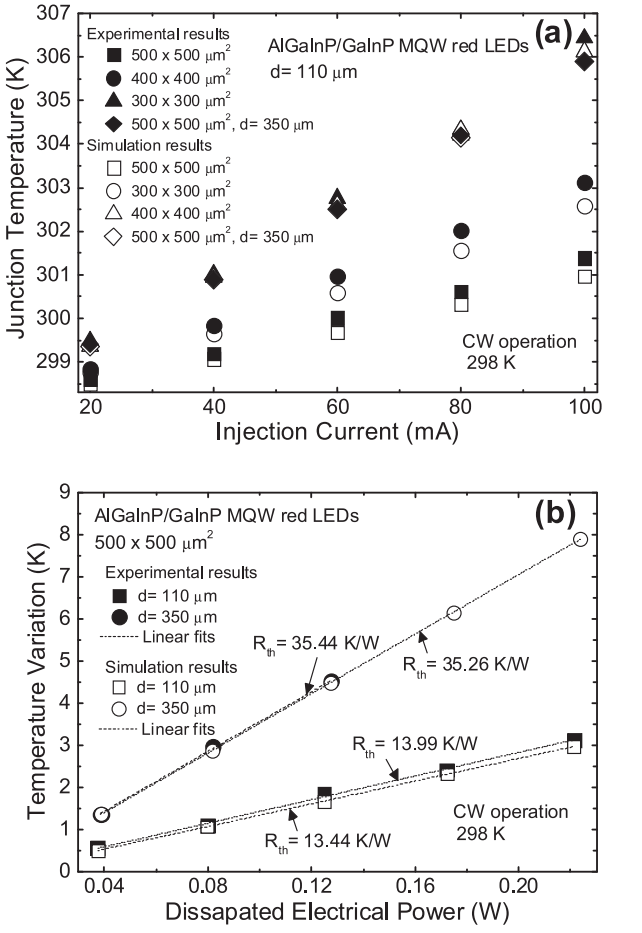

Fig. 6. (a) Measured and simulated junction temperatures versus injection current for LEDs with different chip sizes at 298 K under CW mode and (b) measured and simulated temperature variations versus dissipated electrical power for 500 × 500 μm^2 LEDs with 110 μm and 350 μm thick substrates.

R_{th} values were experimentally estimated as 13.99 K/W and 35.44 K/W for 110 μm and 350 μm thick substrates, respectively. The theoretically calculated R_{th} values were 13.44 K/W and 35.26 K/W for each device, indicating a good agreement.

In addition, the emission peak shift method based on the temperature dependent bandgap energy was used to estimate the T_j and R_{th} values. The temperature coefficient was obtained under pulsed current, and the wavelength shift was measured under pulsed and CW modes. From the experimentally measured data, the T_j value can be estimated by the following equation [23]:

$$T_j = T_0 + \frac{\Delta\lambda}{K_\lambda}, \tag{3}$$

where T_0 is the ambient temperature, $\Delta\lambda$ is the peak wavelength shift, and K_λ is the temperature coefficient. The temperature-dependent peak wavelength for 500 × 500 μm² LEDs with 110 μm and 350 μm thick substrates at 100 mA under pulsed mode with 1 μm pulsed width and 1% duty cycle is shown in Fig. 7a. The peak wavelength was linearly increased with increasing the heatsink temperature, indicating a redshift in peak wavelength. The wavelength shift of LEDs with 350 μm thick substrate was larger than that of LEDs with 110 μm thick substrate. The K_λ values were extracted from the linear fits of the peak wavelength versus heatsink temperature. The K_λ values were 0.137 nm/K and 0.148 nm/K for 110 μm and 350 μm thick substrates, respectively.

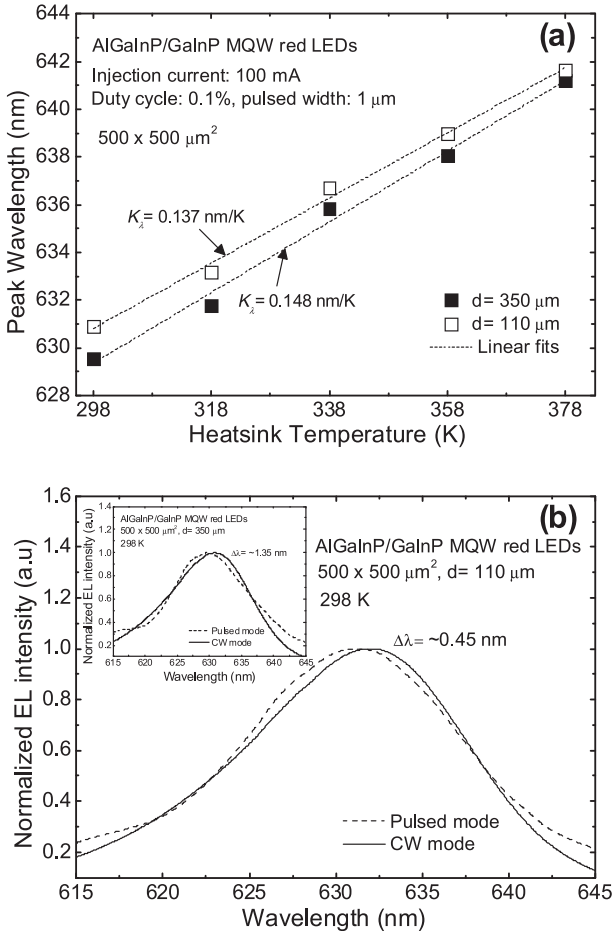

Fig. 7. (a) Temperature-dependent peak wavelength for 500 × 500 μm² LEDs with 110 μm and 350 μm thick substrates at 100 mA under pulsed mode with 1 μm pulsed width and 1% duty cycle and (b) measured normalized EL intensity versus wavelength for the 500 × 500 μm² LED with 110 μm thick substrate at 100 mA and at 298 K in pulsed and CW operations. The inset of (a) shows the EL spectra for 350 μm thick substrate.

Fig. 7b shows the measured normalized EL intensity versus wavelength for the 500 × 500 μm² LED with 110 μm thick substrate at 100 mA and at 298 K in pulsed and CW operations. The inset shows the EL spectra for 350 μm thick substrate. Under pulsed mode, the EL intensity was measured at 100 mA as an initial condition by minimizing the heating effects. The peak wavelength is shifted due to the change of bandgap energy caused by the device heating. Then, it was measured at 100 mA under CW operation. The $\Delta\lambda$ values were determined by the difference of peak wavelength between the pulsed and CW modes. For the substrate thickness of 110 μm, the $\Delta\lambda$ indicated a value of ~ 0.45 nm and it was increased to ~1.35 nm for 350 μm thick substrate. From the measured $\Delta\lambda$ and K_λ values, the T_j was calculated by Eq. (3). Thermal resistance was estimated experimentally by $R_{th} = \Delta T/Q_{heat}$ [24], where ΔT is the temperature difference between the junction temperature and the heatsink (ambient) temperature and Q_{heat} is the dissipated electrical power. Table 2 shows the experimentally determined thermal parameters for 500 × 500 μm² LEDs with 110 μm and 350 μm thick substrates at 298 K under pulsed and CW modes. The injection current is 100 mA. The ΔT values of 3.294 K and 9.112 K were measured at 100 mA for 110 μm and 350 μm thick substrates, respectively. The R_{th} values were also estimated as 14.89 K/W and 40.73 K/W for 110 μm and 350 μm thick substrates, respectively. These values are slightly higher than those obtained by the forward voltage method.

Even for high injection currents, the T_j can be estimated from the R_{th} value. Fig. 8 shows the estimated and simulated junction temperatures of 500 × 500 μm² LEDs with different substrate thicknesses. The experimentally measured results are also shown for comparison. For thicker substrate, the T_j was significantly raised as the injection current was increased. The LED with thinner substrate has better heat removal capability because the heat transfer path was shortened. At high injection current of 450 mA, the T_j of LEDs was estimated from the experimental R_{th} values, which are determined by the forward voltage and peak wavelength shift

Table 2
Experimentally determined thermal parameters for 500 × 500 μm² LEDs with 110 μm and 350 μm thick substrates at 100 mA and at 298 K under pulsed and CW modes.

500 × 500 μm²	Δλ (nm)	K_λ (nm/K)	ΔK (K)	R_{th} (K/W)
d = 110 μm	0.45	0.137	3.294	14.89
d = 350 μm	1.35	0.148	9.112	40.73

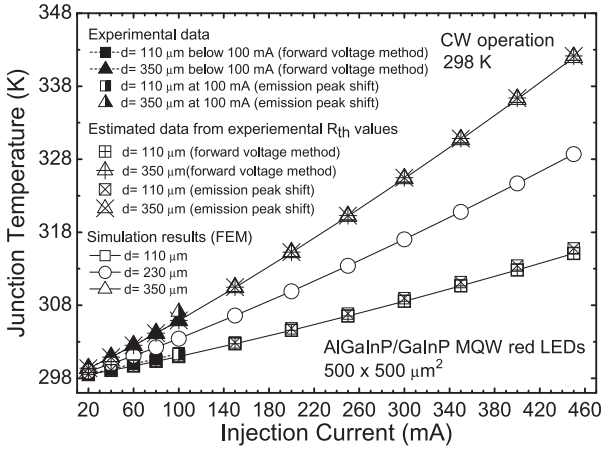

Fig. 8. Estimated and simulated junction temperatures of 500 × 500 μm² LEDs with different substrate thicknesses. For comparison, the experimentally measured results are shown.

methods, as values of ~315 K and ~342 K for 110 μm and 350 μm thick substrates, respectively. The simulated results were fairly consistent with the experimentally measured data by different methods.

4. Conclusion

We investigated the thermal characteristics of the fabricated AlGaInP/GaInP MQW red LEDs by thermal measurements and analysis. For different chip sizes and substrate thicknesses, the *V–I–L* characteristics were experimentally measured. The T_j, which was measured by the forward voltage and emission peak shift methods, was increased with injection current due to the enhanced device heating and it also increased for smaller chip size. Based on the measured *V–I–L* data, the T_j was theoretically calculated using the 3D heat transfer model. The thermal resistance was obtained experimentally and theoretically. The R_{th} values were determined experimentally as values of 13.99 K/W (14.89 K/W) and 35.44 K/W (40.73 K/W) by the forward voltage method (emission peak shift method). From the measured R_{th} values, the T_j was estimated at high injection currents. At 450 mA, the T_j values of 315 K and 342 K were estimated for 500×500 μm^2 LEDs with 110 μm and 350 μm thick substrates, respectively. The use of thinner substrate results in the improved heat removal ability especially at high injection level. The simulation results showed a reasonable consistency with the measured data.

Acknowledgements

This research was supported by Basic Science Research Program through the National Research Foundation of Korea (NRF) funded by the Ministry of Education, Science and Technology (No. 2009-0077580). This work was supported partly by the Technology Innovation Program of the Ministry of Knowledge Economy (2007-F-045-03).

References

[1] Harbers G, Bierhuizen S, Krames MR. Performance of high power light emitting diodes in display illumination applications. J Display Technol 2007;3:98–109.
[2] Steigerwald DA, Bhat JC, Collins D, Fletcher RM, Holcomb MO, Ludowise MJ, et al. Illumination with solid state lighting technology. IEEE J Sel Top Quantum Electron 2002;8:310–20.
[3] Chen NC, Lin CM, Yang YK, Shen C, Wang TW, Wu MC. Measurement of junction temperature in a nitride light-emitting diode. Jpn J Appl Phys 2008;47:8770–82.
[4] Altieri P, Jaeger A, Windisch R, Linder N, Stauss P, Oberschmid R, et al. Internal quantum efficiency of high-brightness AlGaInP light-emitting devices. Appl Phys Lett 2005;98:086101.
[5] Horng RH, Huang SH, Wuu DS, Chiu CY. AlGaInP/mirror/Si light-emitting diodes with vertical electrodes by wafer bonding. Appl Phys Lett 2003;82:4011–3.
[6] Kim T, Leisher PO, Danner AJ, Streubel K, Choquette KD. Photonic crystal structure effect on the enhancement in the external quantum efficiency of a red LED. IEEE Photon Technol Lett 2006;18:1876–8.
[7] Kim SK, Song HD, Ee HS, Choi HM, Cho HK, Lee YH, et al. Metal mirror assisting light extraction from patterned AlGaInP light-emitting diodes. Appl Phys Lett 2009;94:101102.
[8] Song YM, Choi ES, Yu JS, Lee YT. Light-extraction enhancement of red AlGaInP light-emitting diodes with antireflective subwavelength structures. Opt Express 2009;17:20991–7.
[9] Xi Y, Schubert EF. Junction temperature measurement in GaN ultraviolet light-emitting diodes using diode forward voltage method. Appl Phys Lett 2004;85:2163–5.
[10] Murata S, Nakada H. Adding a heat bypass improves the thermal characteristics of a 50 μm spaced 8-beam laser diode array. J Appl Phys 1992;72:2514–6.
[11] Todoroki S, Sawai M, Aiki K. Temperature distribution along the striped active region in high-power GaAlAs visible lasers. J Appl Phys 1985;58:1124–8.
[12] Gu Y, Narendran N. A non-contact method for determining junction temperature of phosphor-converted white LEDs. In: Proc of SPIE, vol. 5187; 2004. p. 107–14.
[13] Nakayama N, Kijima S, Itoh S, Ohata T, Ishibashi A, Mori Y. High-efficiency ZnCdSe/ZnSSe/ZnMgSSe green light-emitting diodes. Opt Rev 1995;2:167–70.
[14] Hatakoshi G, Onomura M, Yamamoto M, Nunoue S, Itaya K, Ishikawa M. Thermal analysis for GaN laser diodes. Jpn J Appl Phys 1999;38:2764–8.
[15] Volz S, Saulnier JB, Chen G, Beauchamp P. Computation of thermal conductivity of Si/Ge superlattices by molecular dynamics techniques. Microelectron J 2000;31:815–9.
[16] Borca-Tasciuc T, Achimov D, Liu WL, Chen G, Ren HW, Lin CH, et al. Thermal conductivity of InAs/AlSb superlattices. Microscale Thermophys Eng 2001;5:225–31.
[17] Piprek J, Yoo SJB. Thermal comparison of long-wavelength vertical-cavity surface-emitting laser diodes. Electron Lett 1994;30:866–8.
[18] Nakwaski W. Thermal conductivity of binary, ternary, and quaternary III–V compounds. J Appl Phys 1988;64:159–66.
[19] Guden M, Piprek J. Material parameters of quaternary III–V semiconductors for multilayer mirrors at 1.55 μm wavelength. Model Simul Mater Sci Eng 1996;4:349–57.
[20] Piskorski L, Sarzała RP, Nakwaski W. Self-consistent model of 650 nm GaInP/AlGaInP quantum-well vertical-cavity surface-emitting diode lasers. Semicond Sci Technol 2007;22:593–600.
[21] Jhou YD, Chen CH, Chuang RW, Chang SJ, Su YK, Chang PC, et al. Nitride-based light emitting diode and photodetector dual function devices with InGaN/GaN multiple quantum well structures. Solid-State Electron 2005;49:1347–51.
[22] Chhajed S, Xi Y, Li YL, Gessmann T, Schubert EF. Influence of junction temperature on chromaticity and color-rendering properties of trichromatic white-light sources based on light-emitting diodes. J Appl Phys 2005;97:054506.
[23] Hong E, Narendran NA. A method for projecting useful life of LED lighting systems. In: Proc of SPIE, vol. 5187; 2004. p. 93–9.
[24] Nakwaski W, Osinski M. On the thermal resistance of vertical-cavity surface-emitting lasers. Opt Quantum Electron 1997;29:883–92.